

Magnetic properties of ion-implanted diamond

R. Höhne^a, P. Esquinazi^{a,*}, V. Heera^b, H. Weishart^b

^a Division of Superconductivity and Magnetism, Institute for Experimental Physics II, University of Leipzig, D-04103 Leipzig, Germany

^b Institute of Ion Beam Physics and Materials Research, Forschungszentrum Rossendorf, P.O. Box 510119, D-01314 Dresden, Germany

Received 24 May 2006; received in revised form 13 September 2006; accepted 18 January 2007

Available online 27 January 2007

Abstract

Single crystalline diamond samples of type IIa were implanted with boron and CVD diamond samples with fluorine or iron ions. Defect rich surface layers extending to a depth of about 300 nm for boron and 1 μm for fluorine and iron were produced by multiple energy implantation. The ion concentrations at the implanted regions were between 30 and 600 ppm for iron and fluorine and 0.5 to 1.5 at.% for boron. In all samples the magnetic properties were dominated by the diamagnetism of pure diamond. The main influence of iron and fluorine implantation on the magnetic properties of diamond is the creation of paramagnetic centres induced by disorder. Whereas diamond implanted with boron at a temperature of 900 °C does not show detectable paramagnetism. After subtraction of the linear background all implanted samples show small ferromagnetic-like loops. Although these signals are clearly above the detection limit and appear to be caused by ferromagnetism, we show that the measured loops are mainly caused by a SQUID artefact. We did not find any evidence for the existence of superconductivity in boron-doped diamond samples prepared under the used conditions.

© 2007 Elsevier B.V. All rights reserved.

Keywords: Diamond; Ion implantation; Magnetic properties; Irradiation effects

1. Introduction

Diamond is an attractive material for research and technical application because of its unique properties, such as its hardness, chemical inertness and high thermal conductivity. However, in the last two decades diamond and diamond-related materials attracted interest due to findings of surprising properties to make them promising materials for electronic applications [1]. Efforts were undertaken to produce these materials in the form of nanostructures, wafers or thin films and to dope them using a broad variety of ions. Talapatra et al. [2] found ferromagnetism (FM) in nanosized diamond particles implanted with nitrogen and carbon ions and explained its occurrence by defect generation. The values of saturation magnetization at room temperature were found to be within 0.9 to 11.5 emu/g in the active volume assuming 80 nm penetration depth. The highest magnetization values were achieved for the nitrogen-doped samples demonstrating the importance of the nature of the implanted species. We note, however, that in that work no

information on the impurity concentration in the samples and the measured values of the magnetic moments were given.

Boron-doped diamond can be interesting for applications in electric devices [3,4]. Whereas lightly boron-doped diamond shows p-type character [5], heavily boron-doped diamond has metallic conduction [6]. Boron in diamond occupies the substitutional site rather than an interstitial site and gives rise to a strong hybridization between B 2p and C 2p when its concentration is small (~ 0.1 at.%) [3]. A metal-insulator transition in boron-implanted diamond was reported by Tshepe et al. [7].

New enthusiasm in the diamond research was generated by the discovery of superconductivity in highly boron-doped diamond. Ekimov et al. [8] prepared boron-doped diamond bulk samples with about (2.8 ± 0.5) at.% boron using high-pressure, high-temperature growth process and reported that this material becomes a type-II superconductor with a critical temperature T_C around 4 K. The corroboration for superconductivity in a heavily boron-doped Chemical Vapour Deposited (CVD) diamond thin film with a T_C between 4.2 and 7.4 K was found by Takano et al. [9]. They observed superconductivity in samples with doping rates as low as 0.18%. Using ultrahigh resolution laser-excited photoemission spectroscopy Ishizaka et al. [10]

* Corresponding author.

E-mail address: esquin@physik.uni-leipzig.de (P. Esquinazi).

observed a superconducting gap evolving below 11 K and discussed the result in terms of a boron-induced disorder effect. Because the incorporation of trivalent impurities like nitrogen, phosphorous or boron into the carbon matrix could lead to ferromagnetism [11], boron implantation into diamond is of actual interest.

The above-mentioned discoveries as well as reports about FM in carbon-based materials [12–17] and theoretical predictions about the existence of ferromagnetism in carbon-based materials induced by disorder [18,19] initialized the present studies. Ion implantation is a powerful tool to produce diamond samples with special properties [20,21]. By implantation of diamond with boron, fluorine or iron our aim was to produce structures with different degrees of lattice damage and to study their magnetic properties. Using a large number of differently implanted samples and high-sensitive SQUID measurements we searched for ferromagnetism or superconductivity in doped diamond. Iron as dopant was chosen due to its large atomic radius and to confirm (or not) some reports about the special role of iron for the creation of ferromagnetism in carbon structures [22,23].

2. Experimental

Single crystalline, ultra-clean natural diamond-IIa samples were used for the implantation with boron (samples B1–B3). Diamond samples prepared by CVD were implanted with fluorine (samples F1(b) and F1(c)) or iron (samples Fe1, Fe2(a)–Fe2(d) and Fe3). The sample area was $3 \times 3 \text{ mm}^2$ and the mass between 7.5 and 9.6 mg (see Table 1). The sample thickness was about 250 μm . The implantations were performed by multi-energy implantation in the ranges of 25 keV–190 keV for boron at 900 °C, 0.4–2.4 MeV for fluorine and 1.0–4.0 MeV for iron at room temperature. The ion depth and damage distribution was determined by SRIM simulation [24]. The thickness (mass) of the implanted region was 300 nm (9.5 μg) for the boron-implanted samples and 1 μm (32 μg) for the iron- and the fluorine-implanted samples. Post-implantation annealing of the boron-implanted samples was carried out in an rf-heated furnace at 1500 °C for 10 min in pure argon ambient. The chemical cleaning of the natural diamond samples after implantation and annealing includes a graphite-etching step in boiling $\text{HNO}_3/\text{H}_2\text{SO}_4$. CVD-diamonds were only cleaned with propanol and acetone in an ultrasonic bath. An overview about all samples used and the implantation conditions are given in Table 1.

Magnetization measurements were carried out using a Superconducting Quantum Interference Device (SQUID) magnetometer (Quantum Design MPMS-7) with a RSO option and a resolution better than 10^{-7} emu. The samples were glued with a small amount of varnish on the middle part of a thin homogeneous quartz stick with a length of about 18 cm. Neither the stick nor the Varnish gave detectable contributions to the magnetic moment. Hysteresis loop measurements at fixed temperatures by cycling the magnetic field between +10 kOe and –10 kOe (or between +2 kOe and –2 kOe) as well as measurements of the temperature dependence of magnetization at different constant magnetic fields after zero field cooling (ZFC) or field cooling (FC) were performed. After each step of

Table 1

Overview of the samples and the conditions of ion implantation and sample treatment

| Sample name | Whole mass (mg) | Total dose | T (implantation) (°C) | Remarks |
|-------------|-----------------|---------------------------------------|-------------------------|--|
| B1(a) | 8.2 | $2.31 \times 10^{16} \text{ B/cm}^2$ | | |
| B1(b) | 8.2 | $2.31 \times 10^{16} \text{ B/cm}^2$ | | B1(a) heated at 1500 °C |
| B1(c) | 8.2 | $2.31 \times 10^{16} \text{ B/cm}^2$ | 900 | $6.93 \times 10^{16} \text{ B/cm}^2$ onto the backside of B1 (b) |
| B1(d) | 8.2 | $2.31 \times 10^{16} \text{ B/cm}^2$ | | B1(c) heated at 1500 °C |
| B2(a) | 7.5 | 0 | – | Virgin sample; IIa |
| B2(b) | 7.5 | $2.31 \times 10^{16} \text{ B/cm}^2$ | 900 | |
| B3(a) | 6.5 | 0 | – | Virgin sample; IIa |
| B3(b) | 6.5 | $2.31 \times 10^{16} \text{ B/cm}^2$ | 900 | |
| B3(c) | 6.5 | $2.31 \times 10^{16} \text{ B/cm}^2$ | 900 | $2.31 \times 10^{16} \text{ B/cm}^2$ onto the backside of B3 (b) |
| F1(a) | 9.5 | 0 | | Virgin sample |
| F1(b) | 9.5 | $1.5 \times 10^{15} \text{ F/cm}^2$ | 23 | |
| F1(c) | 9.5 | $3.0 \times 10^{15} \text{ F/cm}^2$ | 23 | $1.5 \times 10^{15} \text{ F/cm}^2$ onto F1(b) |
| Fe1 | 9.5 | $5.0 \times 10^{14} \text{ Fe/cm}^2$ | 23 | |
| Fe2(a) | 9.6 | $1.5 \times 10^{15} \text{ Fe/cm}^2$ | 23 | |
| Fe2(b) | 9.6 | $3.0 \times 10^{15} \text{ Fe/cm}^2$ | 23 | $1.5 \times 10^{15} \text{ F/cm}^2$ onto Fe2(a) |
| Fe2(c) | 9.6 | $6.0 \times 10^{15} \text{ Fe/cm}^2$ | 23 | $3.0 \times 10^{15} \text{ F/cm}^2$ onto F1(b) |
| Fe2(d) | 9.6 | $1.05 \times 10^{16} \text{ Fe/cm}^2$ | 23 | $4.5 \times 10^{15} \text{ F/cm}^2$ onto F1(c) |
| Fe3 | 8.3 | $5.0 \times 10^{15} \text{ Fe/cm}^2$ | 450 | |
| DNV | 6.8 | 0 | – | Virgin sample; IIa |

The second line gives the mass of the whole diamond sample, where the mass of the implanted region is 9.5 μg for the boron-implanted samples and 32 μg for the iron- and the fluorine-implanted samples. The samples B1 to B3 are natural diamond IIa; all other samples are CVD diamond. The third column contains the total dose of ion implantation including all implantations performed before. When a subsequent implantation was performed on the sample backside, then this dose is written below the first one. After implantation and characterization the samples B1(a) and B1(c) were annealed at 1500 °C for 10 min and then denoted as B1(b) and B1(d), respectively.

implantation or heat treatment the magnetic properties were studied. For all measurements presented here the magnetic field was parallel to the implanted area. All additional measurements with the field out-of-plane confirmed all these results.

The structural properties of the boron-implanted samples (B1(a), B1(b)) were studied by Raman spectroscopy in backscattering geometry using an 100 mW yttrium–aluminum–garnet laser with a wave length of 532 nm and by Fourier transform infrared spectroscopy (FTIR). Hall-effect measurements were done on sample B1(b). For the sample Fe2(a) the iron content was determined by particle induced X-ray emission (PIXE) using protons.

3. Results and discussion

3.1. Structural and elemental characterization

The iron content in an area of 0.5 mm^2 of sample Fe2(a) was determined by PIXE. Assuming 1 μm for the penetration depth

of protons with an energy of 2.25 MeV used for PIXE one obtains an iron content of 300 $\mu\text{g/g}$ in comparison to 390 $\mu\text{g/g}$ for the nominally implanted Fe content. Taking into account that the low electrical conductivity of the diamond sample causes an accumulation of electrical charges on the surface (interfering the penetration of protons used for PIXE) the agreement can be considered as satisfactory.

The depth distributions of ions and damage in the implanted diamond samples were simulated with the computer code SRIM 2003.26 [24]. A displacement energy of 52 eV for vacancy generation in diamond [25] is used for the simulations. Figs. 1 and 2 show the boron concentration and lattice damage (vacancy concentration) per ion dose as function of depth for the samples B1–B3, respectively. The multi-energy implantation (190 keV – 25 keV, see Fig. 1) produces an almost uniform boron-doped region between 40 and 290 nm below the sample surface. Thus, sample B1 (a), which is implanted with $2.31 \times 10^{16} \text{ B}^+/\text{cm}^2$, has a mean boron density of about $9 \times 10^{20} \text{ cm}^{-3}$ (0.5 at.%) in this region. The integral of the damage distribution shown in Fig. 2 gives 94 vacancies (carbon displacements) per boron ion. The maximum vacancy density is about 1×10^{23} for a dose of $2.31 \times 10^{16} \text{ B}^+/\text{cm}^2$. It exceeds clearly the critical damage threshold of 10^{22} cm^{-3} above which damaged diamond converts to graphite upon annealing at moderate temperatures [26]. In order to avoid this effect, the boron implantations were carried out at 900 °C. At such high implantation temperatures rapid vacancy-interstitial recombination considerably reduces the damage [27,20,21]. Analogous simulations yield a penetration depth of about 1 μm for the iron- and the fluorine-implanted samples according to the implantation conditions used.

In order to check whether our implantation condition at elevated temperature was appropriate to avoid graphitization we performed Raman measurements. Raman spectroscopy is a very sensitive tool to detect smallest amounts of graphite in diamond because the Raman intensity of graphite is about 50 times that of diamond. Raman measurements (see Fig. 3) confirm that graphitization of the implanted sample was largely avoided. The implanted and chemically cleaned sample shows a pronounced Raman peak characteristic for diamond at wave number of 1332 cm^{-1} , which would not be visible in the case of graphitic

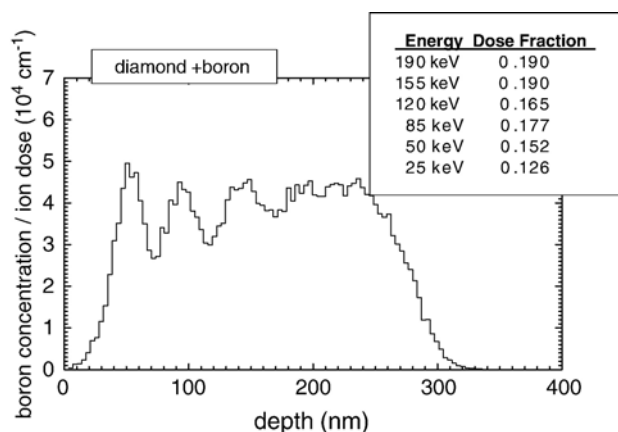


Fig. 1. Calculated depth distribution of boron implanted into diamond by the multi-energy implantation scheme given in the inset.

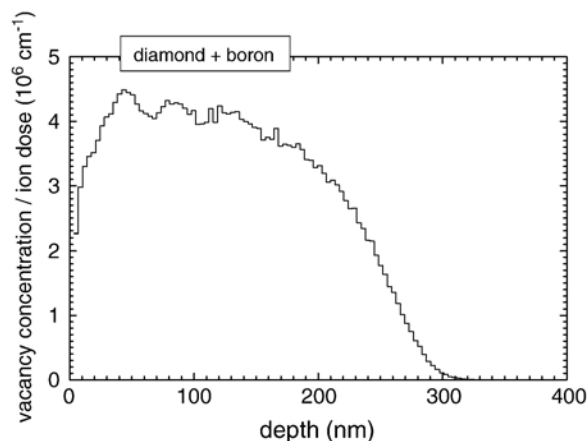


Fig. 2. Calculated depth distribution of vacancies generated by boron multi-energy implantation (see inset in Fig. 1) into diamond.

layer formation. Due to the high optical absorption of a 300 nm thick layer with graphitic bonds the remaining diamond signal from the bulk would be completely hidden in a broad D-band appearing in damaged diamond [20,21]. Moreover, the lack of the G-band around the wave number 1585 cm^{-1} demonstrates that the implanted layer is largely free from graphitic bonds [20,21]. Post-implantation thermal annealing at 1500 °C, necessary for electrical activation of boron as acceptor [7,28], leads to little surface graphitization as indicated by the bump around 1550 cm^{-1} in the Raman spectrum, which completely vanishes after chemical cleaning (see Fig. 3). No boron related signals could be found in the Raman spectrum. Obviously, the Raman spectroscopy is not sensitive enough to detect such a small fraction of boron in diamond. In order to check whether the boron atoms were built in the diamond matrix another method like FTIR must be applied. FTIR is a sensitive method to look for boron–carbon bonds [29,30]. The FTIR spectrum (see Fig. 4) of the implanted sample shows additional modes besides the typical diamond signal [31,32]. The signal around 1180 cm^{-1} can be clearly attributed to a boron–carbon bonding [29,30]. The other signal around 600 cm^{-1} has probably the

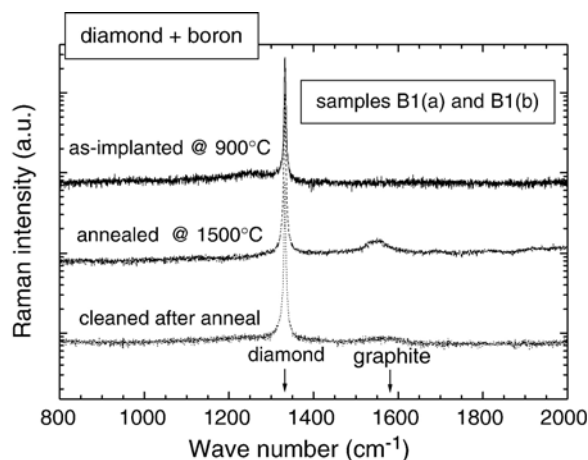


Fig. 3. Raman spectra of boron-implanted diamond (samples B1 (a) and B1(b)). The positions of the signal of undisturbed diamond and graphite are indicated by arrows.

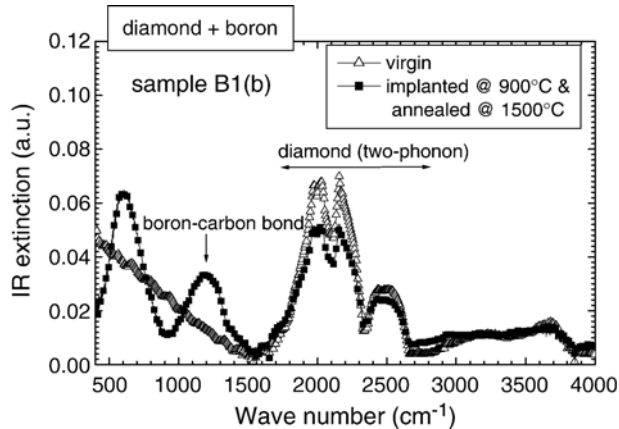


Fig. 4. FTIR spectra of virgin and boron-implanted diamond (sample B1(b)). The characteristic IR band of diamond and the signal of the boron–carbon bond vibration are indicated.

same origin. The large width of the signals obviously comes from a broad scattering of the bonding energies caused by the lattice damage.

A Hall effect measurement of sample B1(b) demonstrates that at least a fraction of the implanted boron atoms is electrically active and must reside therefore on substitutional lattice sites. The Hall effect measurement at room temperature (RT) reveals a hole concentration of $1.7 \times 10^{19} \text{ cm}^{-3}$ and a Hall mobility of $2.2 \text{ cm}^2/\text{Vs}$. It should be noted that at room temperature the hole concentration in boron-doped diamond is smaller by orders of magnitudes than the active acceptor concentration [28] as long as the boron concentration is well below the critical value for the metal-insulator transition. Tshepe et al. [7] found the critical boron concentration in specially prepared diamond samples (CIRA process [33] and final annealing at $1700 \text{ }^\circ\text{C}$) at $3.9 \times 10^{21} \text{ cm}^{-3}$ which is more than 4 times higher than the boron content in the present sample. The resistivity of such a metallic-like diamond sample is below $0.01 \text{ } \Omega \text{ cm}$ at RT. Our sample prepared by implantation of boron at $900 \text{ }^\circ\text{C}$ has a resistivity of $0.17 \text{ } \Omega \text{ cm}$. These numbers indicate that this sample is not at the metal-insulator transition but closely below the threshold. For comparable boron concentrations the hot implantation process appears to be more effective for acceptor activation than the CIRA process applied by Tshepe et al. [7]. They found a clearly higher resistivity of about $8 \text{ } \Omega \text{ cm}$ for a diamond sample doped with 10^{21} boron/ cm^3 although it was annealed at $1700 \text{ }^\circ\text{C}$.

3.2. Magnetic characterization

For all samples registered in Table 1 measurements of the magnetic moment as a function of the temperature between 2 K and 300 K at different constant magnetic fields after ZFC or FC were performed. Fig. 5 shows some typical examples for boron, fluorine and iron-implanted samples and a virgin sample. In spite of some differences in the sample mass in all figures the magnetic moment and not the magnetization values were used for a better distinction of the curves and to show the order of magnitude of the raw data. In the temperature region above

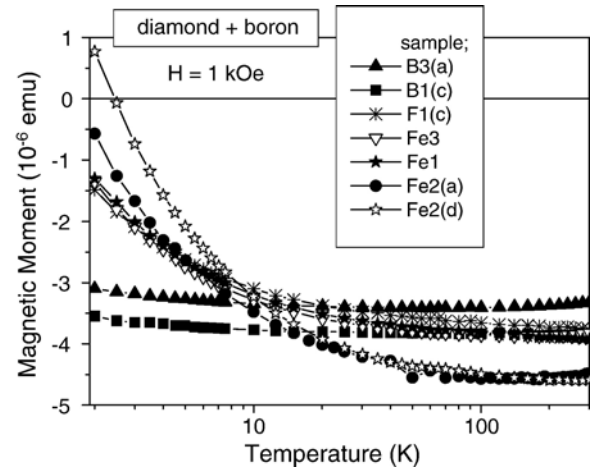


Fig. 5. Magnetic moment in units of 10^{-6} emu as a function of the temperature between 2 K and 300 K measured at a constant magnetic field $H=1 \text{ kOe}$ after ZFC from 300 K to 2 K for several ion-implanted diamond samples.

100 K the temperature-independent diamagnetism of diamond clearly dominates. In the low temperature region the behaviour is characterized by a superposition of diamagnetism and paramagnetism, the latter being strongly influenced by the ion implantation. Fig. 6 shows the magnetic moment over the reciprocal temperature. At low temperatures the paramagnetic part of the magnetic moment for all measured samples follows the classical Curie law of paramagnetism. The slopes of the curves for the virgin sample (B3(a)) as well as for all boron-implanted samples are very small, see Fig. 6. In contrast, the fluorine- and iron-implanted samples show a clear increase of the paramagnetic contribution with the dose of implantation. In the sample with the highest iron content the sign of the magnetic moment at $T=2 \text{ K}$ is even positive. Using the Curie law and the slope of the linear part of the $m(1/T)$ curves the total number of (single) Bohr magnetons μ_B were calculated for all samples used and drawn in Fig. 7 as a function of the number of ions (dose multiplied with the sample area) implanted in the whole sample. Within experimental uncertainty the boron-implanted samples show no change in the number of paramagnetic centres

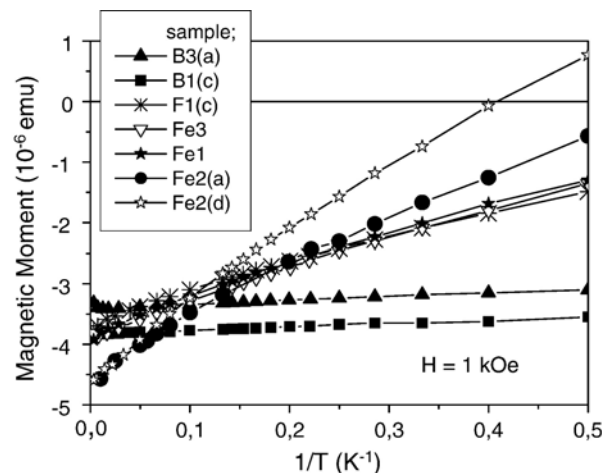


Fig. 6. Shows the magnetic moment for the same samples of Fig. 5, but as a function of the reciprocal temperature.

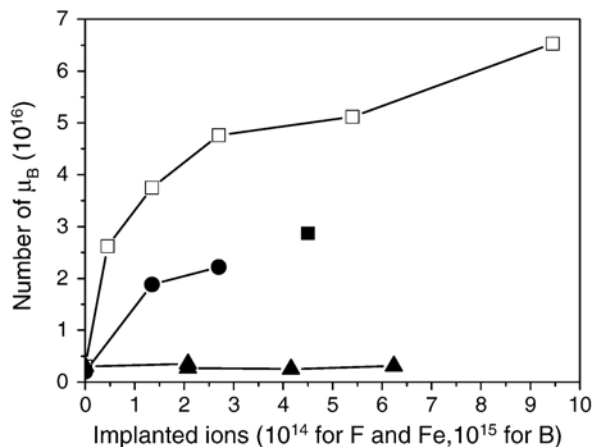


Fig. 7. The total number of Bohr magnetons μ_B in the sample in units of 10^{16} as a function of the total number of the implanted ions in the sample in units of 10^{14} for iron (open and full squares for implantations at room temperature and $450\text{ }^\circ\text{C}$, respectively) and fluorine (full circles) and 10^{15} for boron-implanted at $900\text{ }^\circ\text{C}$ (full triangles).

as a function of boron content in comparison with the virgin sample. Heat treatments performed at $1500\text{ }^\circ\text{C}$ do not change this behaviour. This speaks for a small lattice damage of all boron-implanted samples due to recombination processes during the high-temperature implantation.

In the fluorine- and iron-implanted samples the number of paramagnetic centres clearly increases with the dose and is much higher than the number of implanted ions. This is in agreement with the SRIM simulations which yield 423 and 2440 for the number of vacancies (displacements of C atoms) per implanted fluorine and iron ion, respectively. The expected contribution of the iron ions to the observed paramagnetism – independent of the assumed number of μ_B per iron ion – is very small in comparison with the measured paramagnetism. This result clearly indicates the creation of paramagnetic centres caused by the lattice damage produced by the ion implantation. The higher effect of iron in comparison with that of fluorine on the degree of damage is probably caused by its higher ion radius and the higher implantation energy. A rough indication of the degree of damage is the change of sample colour caused by optically active defects visible in all F- and Fe-implanted diamond samples. From Fig. 7 is seen that the higher the implantation dose the higher the number of μ_B , however there is no linear proportionality. The slope of the curves in Fig. 7 (for F- and Fe-implanted samples) decreases with increasing dose. Such behaviour can be explained by the non-linear damage built-up known from high-dose ion implantation into semiconductors [34,35]. O’Raifeartaigh et al. [35] demonstrated for MeV Ni implantation into silicon that the areal concentration of paramagnetic centres clearly exceeds the ion dose and has a sublinear dose dependence if the implantation temperature is smaller than 350 K . In the case of implantations performed at higher temperatures ($900\text{ }^\circ\text{C}$ for diamond with boron and $450\text{ }^\circ\text{C}$ for sample Fe3) the degree of recombination processes during the implantation is much higher and therefore the number of paramagnetic centres is smaller than that of samples implanted at room temperature as can be seen in Fig. 7.

For the majority of the samples the temperature dependence of the magnetic moment was measured after ZFC and FC. Within experimental uncertainty both curves coincide for all samples. Special efforts were done for all boron-implanted samples in order to search for the possible occurrence of superconductivity. In all $m(T)$ curves no differences between ZFC and FC curves could be detected down to 2 K , using magnetic fields $H=10, 100$ and 1000 Oe . Although the low field values under normal conditions are not suitable to get well-defined SQUID signals in our samples with such small magnetic moments, these fields would be enough to detect the expected negative moments if after ZFC below the transition temperature superconductivity would exist. No indications for superconductivity were found from these measurements neither in samples with $2.31 \times 10^{16}\text{ B/cm}^2$ (or $9.2 \times 10^{20}\text{ B/cm}^3$, i.e. $0.5\text{ at.}\%$) nor in the samples B1(c) and B1(d) with additional $6.93 \times 10^{16}\text{ B/cm}^2$ (or $2.7 \times 10^{21}\text{ B/cm}^3$, i.e. $1.5\text{ at.}\%$) on the sample backside. It is worth to note that the boron concentrations of these samples are similar to those samples where superconductivity was detected (0.18 to $0.53\text{ at.}\%$ in [9] and $2.8\text{ at.}\%$ in [8]). The heat treatments of the as-implanted samples B1(a) and B1(c) at $1500\text{ }^\circ\text{C}$ (denoted as B1(b) and B1(d), respectively) did not change the measured behavior. It can be speculated that insufficient boron activation due to implantation

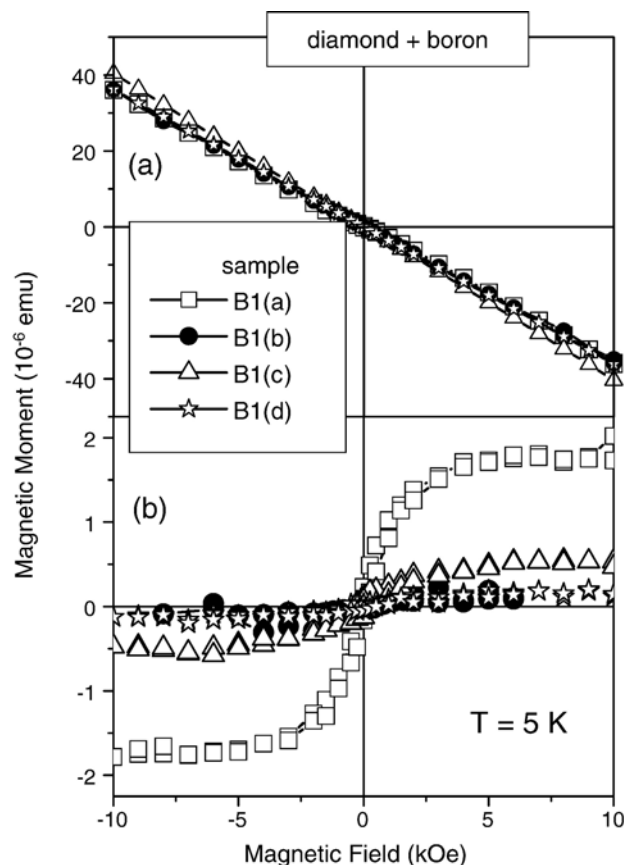


Fig. 8. Magnetic moment in units 10^{-6} emu at $T=5\text{ K}$ as a function of the magnetic field cycled between $+10\text{ kOe}$ and -10 kOe for a boron-implanted diamond sample after two boron implantations (B1(a) and B1(c)) and following heat treatments at $1500\text{ }^\circ\text{C}$ (B1(b) and B1(d)); (a): without any subtraction, (b): after subtraction of the diamagnetic (linear) background.

defects [33] or the lack of boron–boron-pairs prevents superconductivity in our samples (compare Ref. [5] cited in Ref. [10]).

In order to search for the existence of possible ferromagnetic (or superconducting) correlations a large amount of hysteresis loops by cycling the magnetic field were measured at various temperatures between 2 K and 300 K. As an example Fig. 8a shows the magnetic moment of sample B1 as a function of the magnetic field between -10 kOe and $+10$ kOe measured after each step of treatment (a) to (d), see Table 1. In all four cases the field dependence of the magnetic moment is mainly characterized by a linear behaviour caused by the clear diamagnetism of diamond. Therefore the differences between the curves are relatively small.

In order to reveal any ferromagnetic (or superconducting) states in the samples the linear diamagnetic background must be subtracted. Fig. 8b shows the remaining loops after subtraction of the corresponding diamagnetic backgrounds. Weak s-formed ferromagnetic-like loops with saturation at high fields and a small remanence can be observed. We will show later that there is no correlation between the occurrence of these loops and the implantations or treatments of the samples. It seems that the most pronounced loop is observed for the sample after the first boron implantation. The “saturation magnetization” related to the whole sample mass (8.2 mg) is very small: 2.2×10^{-4} emu/g. If the s-loop would be caused by the boron implantation, which is in a depth of ~ 300 nm, then we have to take only a mass of $9.5 \mu\text{g}$ of the implanted region. In this case the saturation magnetization would be ~ 0.19 emu/g. After the first heat treatment the magnetic moment at saturation decreases to $1 \dots 2 \times 10^{-7}$ emu; this is of the order of the uncertainty of our SQUID measurements. To increase the observed effect the next implantation in this sample was performed with the threefold boron dose (B1(c)). The remaining ferromagnetic-like loop was clearly smaller than that after the first implantation. After heat treatment exactly the results after the first heat treatment (B1(b)) were reproduced.

Two additional samples B2 and B3 were measured before and after boron implantation. After subtraction of the diamagnetic background the virgin samples show rest loops of the order of the measuring uncertainty. After boron implantation s-like loops, similar, but smaller than that of sample B1 were measured. We note that for all three boron-implanted samples B1, B2 and B3 the values of the saturation moments of the loops show practically no temperature dependence in the range between 2 K and 300 K.

Fig. 9 demonstrates the typical magnetic behaviour for some selected fluorine- and iron-implanted diamond samples. As for all other diamond samples the main contribution to the magnetic moment comes from the diamagnetism, which is superimposed with the paramagnetic contribution mainly caused by the lattice damage created by the ion implantation. After subtraction of the linear background s-like loops with saturation at high fields and a minor hysteresis can be observed as Fig. 9 shows. These effects are small and of the same order of magnitude as those in boron-implanted samples. In a formal way one could conclude that the saturation magnetic moment m_s increases with fluorine

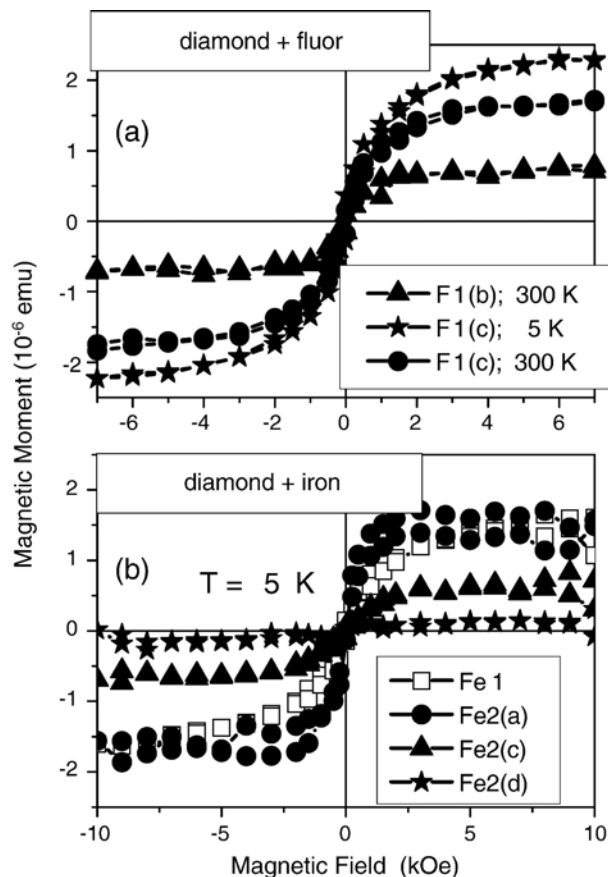


Fig. 9. Magnetic moment in units of 10^{-6} emu after subtraction of the diamagnetic (linear) background measured as a function of the magnetic field cycled between $+7$ kOe and -7 kOe for samples with fluorine (a) and $+10$ kOe and -10 kOe (b) for samples with iron.

content in the used region (see Fig. 9(a)) and has a maximum in the iron-implanted diamond samples for doses between 5.0×10^{14} Fe/cm² and 1.5×10^{15} Fe/cm². In samples with higher Fe contents m_s seems to be clearly smaller. The sample with the highest iron concentration shows only a FM-like effect within the order of the uncertainty of the measurements. The sample Fe3 was implanted at 450°C with similar iron content as sample Fe2(c) in order to test whether a clustering of iron or iron oxide can be achieved and the ferromagnetism can be increased or not. The loops are even smaller than those of sample Fe2(c). In the following we will see that the differences between the loops are arbitrary and not related to a true sample effect.

In the case of observations of new and small effects one has the responsibility to intensively check whether these findings are true and not related to artifacts. We performed additional experiments and repeated several measurements varying the conditions. In the Figs. 10 and 11 two examples of the obtained results are presented. With the aim to increase a possible FM-like effect the sample B3(b) was additionally implanted on the backside with the same boron-dose as for the first side and denoted as sample B3(c) (see Table 1). One would expect an increase of the s-like effect by a factor of 2. However, Fig. 10 shows that between the loops of samples B3(b) and B3(c) there is almost no difference. This result shows that the loop can not

be caused by the implantation. In another experiment a new virgin diamond IIa sample (DNV) and the sample B3(c) were measured first separately and afterwards glued together, see Fig. 11. Whereas the magnetic moment of the ensemble, as expected, is the sum of those of the single samples, the corresponding loop after subtraction of the diamagnetic contribution is clearly smaller than those of the loop of the single sample B3(c). Repeats of measurements, especially a new fixing of the sample on the sample holder led to a change of the intensity of the s-like loops.

If one takes (incorrectly) the implanted region as the magnetically active volume with a penetration depth of 300 nm for diamond with boron and 1 μm for diamond with fluorine or iron, respectively, then the maximum values of the “saturation magnetization” would be about 0.67 emu/cm^3 for boron-implanted and about 0.2 emu/cm^3 for fluorine- or iron-implanted samples. Because of the small volume assumed for the calculation of the magnetization the apparent induced ferromagnetism appears to be not so small.

We may speculate on two possible origins for this artefact: a) The paramagnetic part of the magnetization induced by the implantation, which is not exactly linear with field according to the Langevin relation, could produce s-like loops after a formal subtraction of a linear part. This nonlinearity should be clearly stronger in the low-temperature region. In our samples, however, almost no temperature dependence of the intensity of the loops was observed. b) A nonlinearity of the applied magnetic field as origin of the observed effect can be excluded, because there is no correlation between the saturation magnetic moment values and the slope of the $m(H)$ curves. Actually quite the opposite, in samples with higher magnetic moments smaller or no s-like loops were measured. From our measurements we conclude that the artefact observed (only) in samples with small total magnetic (when the slope of the $m(H)$ curves is of the order of some 10^{-9} emu/Oe) can come from not well behaved SQUID signals, probably caused by a non-central, vertical or lateral

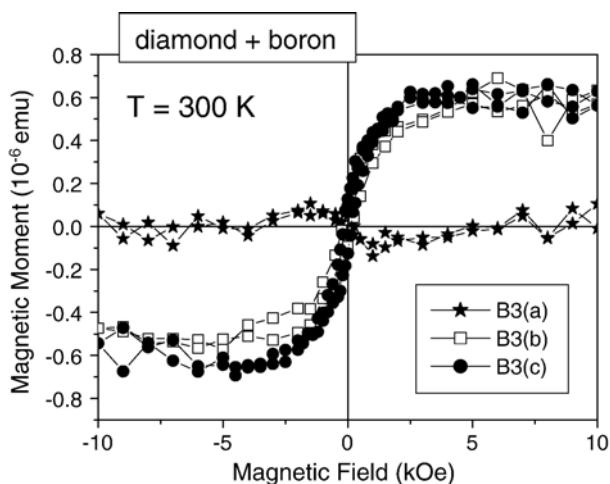


Fig. 10. Magnetic moment in units of 10^{-6} emu after subtraction of the diamagnetic (linear) background measured as a function of the magnetic field for the virgin sample B3(a) and the same sample after additional boron implantation on one side (B3(b)) and additionally on the other side (B3(c)).

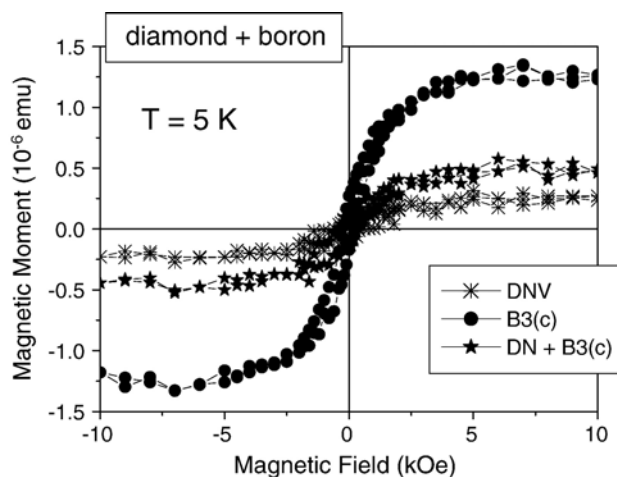


Fig. 11. Magnetic moment in units of 10^{-6} emu after subtraction of the diamagnetic (linear) background measured as a function of the magnetic field for a virgin diamond of type IIa and the boron-implanted sample (B3(c)) as well as for both samples glued together.

position of the sample inside the superconducting detection coils.

4. Summary and conclusions

Implantation of fluorine or iron ions in diamond samples at room temperature produced a lattice disorder and an enhancement of paramagnetic centres. The number of atomic displacements estimated by SRIM simulations and the number of Bohr magnetons determined from the temperature dependence of the magnetization were much larger than the number of implanted ions. The disorder leads to a paramagnetic contribution to the magnetization, increasing with the number of implanted ions. In contrast boron implantation performed at $900 \text{ }^\circ\text{C}$ and at lower energies produces less lattice damage and almost no paramagnetic contribution to the magnetization. In spite of high concentration of implanted boron we did not find any indication for superconductivity for $T \geq 2 \text{ K}$.

For all samples the magnetic properties were dominated by diamagnetism of diamond, which is superimposed to the paramagnetism in fluorine- and in iron-implanted samples. After subtraction of the linear background in the field dependence of the magnetic moment small s-like loops remained with only a small hysteresis in all implanted samples. These effects are small, but in most samples clearly above the detection limit of the SQUID magnetometer. Although the s-like loops appear to be real ferromagnetic loops, we could show that these loops are caused by a SQUID artefact, which produces a small deviation from the real linear dependence of the magnetic moment on magnetic field. Our work shows clearly that one has to be sceptical when in the literature ferromagnetic magnetization is reported without information about the real measured magnetic moments and the volume or mass of samples and without discussion of possible artefacts.

Another interesting result is that iron as a magnetic ion does not play any special role for the magnetic properties in implanted diamond samples. In the sample with the highest iron

concentration the ratio between carbon and iron atoms in the implanted region is about 1700:1. This means that 12 C-atoms are between two Fe-atoms. An interaction between iron atoms over such a relative long distance is unlikely and we did not find any indication for an interaction between carbon and iron, which results in ferromagnetism. In the case of boron implantation the aim was to produce a diamond layer where the majority of the boron ions are situated on substitutional places. As can be seen from the magnetization measurements the degree of disorder in these samples is low. Despite the concentration of boron ions in the implanted diamond layer is high enough to produce superconductivity, according to Refs. [8] and [9], we did not find any indications for this phenomenon. Whether the electrical activity of boron ions is not high enough in our samples or other causes are responsible for the lack of superconductivity is not yet clear and will be investigated in the future. In summary, there is no indication for superconductivity or ferromagnetism in all implanted diamond samples.

Acknowledgements

The authors thank D. Spemann for the PIXE measurement on one sample. This work was supported by the European project “Ferrocabon”.

References

- [1] M. Willander, M. Friesel, Q. Wahab, B. Straumal, *J. Mater. Sci., Mater. Electron.* 17 (2006) 1.
- [2] S. Talapatra, P.G. Ganesan, T. Kim, R. Vajtai, M. Huang, M. Shima, G. Ramanath, D. Srivastava, S.C. Deevi, P.M. Ajayan, *Phys. Rev. Lett.* 95 (2005) 0997201.
- [3] G.S. Gildenblat, S.A. Grot, A. Baldzian, *Proc. IEEE* 79 (1991) 647.
- [4] J. Nakamura, E. Kabasawa, N. Yamada, Y. Einaga, D. Saito, H. Isshiki, S. Yugo, R.C.C. Perera, *Phys. Rev., B* 70 (2004) 245111.
- [5] J.W. Glesener, *Appl. Phys. Lett.* 64 (1994) 217.
- [6] H. Shimomi, Y. Nishibayashi, N. Fujimori, *Jpn. J. Appl. Phys., Part 1* 30 (1991) 1363.
- [7] T. Tshepe, C. Kasl, J.F. Prins, M.J.R. Hoch, *Phys. Rev., B* 70 (2004) 245107.
- [8] E.A. Ekimov, V.A. Sidorov, E.D. Bauer, N.N. Mel'nik, N.J. Curro, J.D. Thompson, S.M. Stishov, *Nature* 428 (2004) 542.
- [9] Y. Takano, M. Nagao, I. Sakaguchi, M. Tachiki, T. Hatano, K. Kobayashi, H. Umezawa, H. Kawarada, *Appl. Phys. Lett.* 85 (2004) 2851.
- [10] K. Ishizaka, R. Eguchi, S. Tsuda, T. Yokoya, T. Kiss, T. Shimojima, T. Togashi, S. Watanabe, C.-T. Chen, C.Q. Zhang, Y. Takano, M. Nagao, I. Sakaguchi, H. Kawarada, S. Shin, *Phys. Rev. Lett.* 98 (2007) 047003.
- [11] T.L. Makarova, *Studies of High-temperature Superconductivity*, NOVA Science Publishers, Inc., New York, 2003, p. 107.
- [12] K. Murata, H. Ushijima, H. Ueda, K. Kawaguchi, *J. Chem. Soc., Chem. Commun.* (1991) 1265.
- [13] P. Turek, K. Nozawa, D. Shiomi, K. Awaga, T. Inabe, Y. Maruyama, M. Kinoshita, *Chem. Phys. Lett.* 180 (1991) 327.
- [14] P.M. Allemand, K.C. Khemani, A. Koch, F. Wudl, K. Holczer, G. Donovan, G. Grüner, J.D. Thompson, *Science* 253 (1991) 301.
- [15] T. Murakami, H. Suematsu, *Pure Appl. Chem.* 68 (1996) 1463.
- [16] P. Esquinazi, A. Setzer, R. Höhne, C. Semmelhack, Y. Kopelevich, D. Spemann, T. Butz, B. Kohlstrunk, M. Lösche, *Phys. Rev., B* 66 (2002) 024429.
- [17] P. Esquinazi, R. Höhne, *J. Magn. Magn. Mater.* 290–291 (2005) 20.
- [18] A.A. Ovchinnikov, I.L. Shamovsky, *J. Mol. Struct., Theochem* 251 (1991) 133.
- [19] J. González, F. Guinea, M. Vozmediano, *Phys. Rev., B* 63 (2001) 134421.
- [20] H. Weishart, V. Heera, F. Eichhorn, B. Pecz, A. Barna, W. Skorupa, *J. Appl. Phys.* 94 (2003) 1195.
- [21] H. Weishart, F. Eichhorn, V. Heera, B. Pecz, A. Barna, W. Skorupa, *J. Appl. Phys.* 98 (2005) 043503.
- [22] C.-Ch. Mertins, S. Valencia, W. Gudat, P.M. Oppeneer, O. Zaharko, H. Grimm, *Europhys. Lett.* 66 (2004) 743.
- [23] J. Coey, M. Venkatesan, C. Fitzgerald, A. Douvalis, I. Sanders, *Nature* 420 (2002) 156.
- [24] J.F. Ziegler, J.P. Biersack, U. Littmark, *The Stopping and Range of Ions in Solids*, Pergamon, New York, 1985, www.SRIM.org.
- [25] D. Saada, J. Adler, R. Kalish, *Int. J. Mod. Phys. C* 9 (1998) 61.
- [26] C. Uzan-Saguy, C. Cytermann, R. Brener, V. Richter, M. Shaanan, R. Kalish, *Appl. Phys. Lett.* 67 (1995) 1194.
- [27] S. Praver, R. Kalish, *Phys. Rev., B* 51 (1995) 15711.
- [28] F. Fontaine, C. Uzan-Saguy, B. Philosoph, R. Kalish, *Appl. Phys. Lett.* 68 (1996) 2264.
- [29] K. Shirai, S. Emura, S. Gonda, Y. Kumashiro, *J. Appl. Phys.* 78 (1995) 3392.
- [30] R. Gago, et al., *J. Appl. Phys.* 92 (2002) 5177.
- [31] Mc Namara, et al., *JAP* 76 (1994) 2466.
- [32] H. Orpychal, et al., *Diamond Relat. Mater.* 6 (1997) 940.
- [33] J.F. Prins, *Phys. Rev., B* 38 (1988) 5576.
- [34] J.K.N. Lindner, R. Domres, E.H. Te Kaat, *Nucl. Instrum. Methods Phys. Res., B Beam Interact. Mater. Atoms* 39 (1989) 306.
- [35] C. O’Raifeartaigh, R.C. Barklie, J.K.N. Lindner, *Nucl. Instrum. Methods Phys. Res., B Beam Interact. Mater. Atoms* 217 (2004) 442.